This article has been accepted for publication in a future issue of this journal, but has not been fully edited. Content may change prior to final publication. Citation information: DOI 10.1109/TAP.2021.3102112, IEEE Transactions on Antennas and Propagation

Communication

Paraffin-Based RF Microsystems for Millimeter Wave Reconfigurable Antennas

Behnam Ghassemiparvin, *Member, IEEE*, and Nima Ghalichechian, *Senior Member, IEEE*

***Abstract*—We report the design, fabrication, and testing of a millimeter wave reconfigurable antenna based on paraffin phase change material (PCM) variable capacitors. Paraffin is a low loss dielectric ($\tan\delta = 6.6 \times 10^{-4}$ at 100 GHz) that undergoes a 15% volumetric change through its solid-liquid phase change. A RF electro-thermo-mechanical actuator is monolithically integrated with a slot antenna in order to achieve a frequency reconfiguration at 100 GHz. RF performance is verified using on-wafer probing and compared with full-wave and multiphysics simulations. Measured bandwidth of 94.1–104.1 GHz and the resonance frequency shift of 6.8 GHz is achieved. With a maximum voltage of 5.4 V, paraffin based electro-thermo-mechanical actuators has a maximum displacement of 1.4 μm which yielded a 15.3% capacitance change. Using a fully-coupled multiphysics simulation switching time of the actuator is estimated as 5.7 ms. This work is the first demonstration for the new class of low-loss reconfigurable RF microsystem that will enable applications including wireless communication, radars and biomedical sensing.**

***Index Terms*—Millimeter wave (mmW), paraffin, phase change material, reconfigurable antenna, slot antenna.**

I. Introduction

THE recent advent of media-rich mobile devices has increased the demand for high data-rate wireless millimeter-wave (mmW) communications. Such systems, with their very high bandwidth in the frequency range of 30–300 GHz can accommodate this rapid increase in traffic volume. The advent of both the Internet of Things and the increasing number and volume of connected devices has made data traffic both random and diverse. The introduction of frequency, polarization or pattern diversity, through multiple-input-multiple-output (MIMO) systems also increases the capacity of an mmW communication system. Currently, full potential of MIMO performance is not realized in mmW systems due to the limited radio frequency (RF) chains and sparse communication channel [1]. Reconfigurability and adaptability offer an additional degree of freedom for millimeter-wave communication systems to achieve optimal transmission. Using single reconfigurable antenna it is possible to meet various radiation pattern, frequency, and polarization requirements without increasing the number of elements and the associated radio frequency (RF) chains. We note that the realization of reconfigurable antennas at the mmW band provides significant challenges in the design, fabrication, and testing steps.

This work was supported in part by the U.S. National Science Foundation under Grant 1408228.

B. Ghassemiparvin was with the Electroscience Lab, Department of Electrical and Computer Engineering, The Ohio State University, Columbus, OH 43212 USA (e-mail: ghassemiparvin.1@osu.edu). He is now with Apple Inc. Cupertino, CA 95014 USA.

N. Ghalichechain was with the Electroscience Lab, Department of Electrical and Computer Engineering, The Ohio State University, Columbus, OH 43212. He is now with the School of Electrical and Computer Engineering, Georgia Institute of Technology, Atlanta, GA 30332 (nghalich3@gatech.edu).

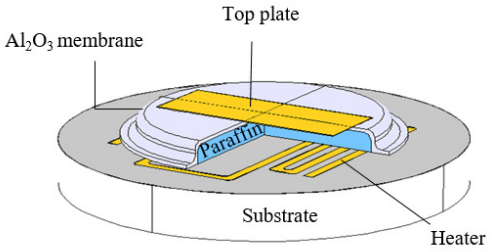

Fig. 1. 3D schematic of the paraffin PCM actuator with integrated heater.

Altering the current distribution of an antenna makes it possible to reconfigure the radiation characteristics and input impedance. Various methods are used for such configuration: electrically tunable elements such as PIN diodes [2]–[5] , varactors [6], [7], Gallium-Arsenide (GaAs) switches [8], and RF micro-electro-mechanical systems (MEMS) [9], [10]. Alternatively, it is possible to achieve reconfiguration by using electrically tunable dielectric materials such as liquid crystals [11], [12] and barium strontium titanate (BST) [13] can also be used.

Paraffin or alkane is a mechanical phase change material (PCM) with a 15% density change over the solid-to-liquid phase transition [14], [15]. Theromechanical actuators based on paraffin can simultaneously provide a large force and displacement [16]–[18]. In addition, the non-polar molecular structure of paraffin yields a low dielectric loss of 6.3×10^{-4} at 110 GHz [19] which facilitates the development of low loss RF components.

Using this unique combination of features, in this paper we detail our development of a slot antenna with two low loss paraffin-based variable capacitors to achieve a frequency reconfiguration at 100 GHz. The basic operation of this paraffin PCM based variable capacitor, a 3D schematic of which is shown in Fig. 1, is as follows: A DC voltage is first applied to the integrated heater to provide the electro-thermal actuation. The generated heat then increases the temperature of the paraffin, with the resulting phase change from solid to liquid. Consequently, volume expansion of the paraffin provides the force to move the top plate of the capacitor. By loading the slot antenna with these capacitors, we can vary both the capacitance and the propagation constant along the slot line to achieve a resonance frequency shift. We base this concept upon our previously published design variations and preliminary simulation results [20]–[22].

This article has been accepted for publication in a future issue of this journal, but has not been fully edited. Content may change prior to final publication. Citation information: DOI 10.1109/TAP.2021.3102112, IEEE Transactions on Antennas and Propagation

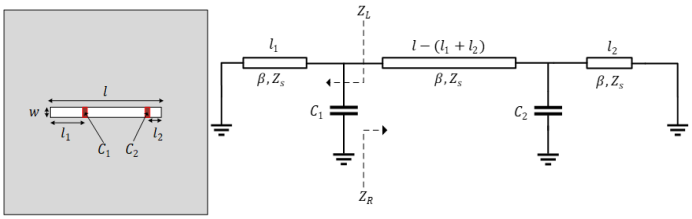

(a) (b)

Fig. 2. (a) Schematic of a loaded slot antenna and (b) equivalent transmission line model.

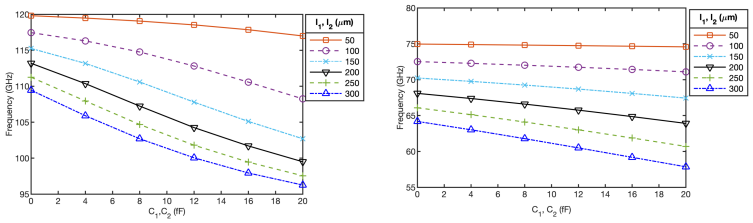

(a) (b)

Fig. 3. Calculated (a) first and (b) second resonance frequencies of the slot antenna with the length of 1357 μm, width of 80 μm fabricated on a 200 μm-thick quartz substrate with relative dielectric constant of 3.8.

This work is the first demonstration of the paraffin-based reconfigurable mmW antenna that is capable of continuous tuning. The proposed paraffin based reconfigurable PCM capacitors offers a viable solution for low loss, monolithically integrated devices that could realize reconfigurable antennas at mmW frequencies. In our previous work [23], MEMS design of the paraffin PCM capacitor, mechanical and thermal challenges of the device is discussed. In addition full description of the microfabrication process and the multiphysics simulation of the electro-thermo-mechanical actuation is presented [23]. On the other hand, in this paper, we have focused on the the antenna design, feeding structure, and the integration of the paraffin PCM capacitors with the mmW slot antenna. In addition, RF characterization of the variable capacitor integrated with the antenna is performed. Moreover, the effects of the microfabrication tolerances and the mechanical performance of the device on the electromagnetic losses and the reconfigurability is addressed.

II. Reconfigurable Slot Antenna Design

To determine the physical dimension of antenna, capacitance values and location, we used a transmission line model of the antenna. Using this model, resonance frequency of the antenna is calculated and the capacitors value and location was optimized to achieve maximum frequency shift with respect to capacitance change.

A. Circuit Model and Optimization of Loaded Slot Antenna

A narrow slot antenna can be modeled as a transmission line shorted at two ends. This circuit is at resonance when the length of the slot is $l = n\frac{\lambda}{2}$ where $n = 1, 2, 3, \ldots$ [24]. Loading this transmission line with two capacitors increases the capacitance and the propagation constant along the line. Consequently, electrical length of the antenna increases and the resonance frequency decreases [7], [25], [26]. Similar to [25], [26], the transmission line model of the loaded slot antenna is used as shown in Fig. 2. Using the circuit model, we then calculate the resonance frequency of the antenna by applying the transverse resonance condition [27]. Using similar analysis to [26], the resonance frequency of the loaded slot antenna is calculated which are dependent on the capacitor values and their location.

Our objective is to maximize the frequency shift with respect to the capacitance ratio of 1.15. This capacitance ratio is determined according to the 15% volumetric change of paraffin. Due to the symmetric structure of the antenna, here it is assumed that $l_1 = l_2$ and $C_1 = C_2$. Optimization procedure is applied for a slot antenna with the length of 1357 μm and the width of 80 μm fabricated on a 200 μm-thick quartz substrate with relative dielectric constant of 3.8. For the capacitance range of $0 \leq C_1 = C_2 \leq 20$ fF, we vary the position of capacitors in the range of 50 μm $\leq l_1 = l_2 \leq 300$ μm. The calculated resonance frequencies are shown in Fig. 3.

According to Fig. 3(a), maximum rate of change for the first resonance is 0.32 GHz/fF which occurs at $l_1 = l_2 = 300\,\mu$m. The rate of change for the second resonance frequency is given in Table I where maximum rate of 1.39 GHz/fF is achieved for $l_1 = l_1 = l_2 = 200\,\mu$m. As the rate of change for second resonance frequency is significantly higher than the first, we consider only the second resonance frequency for the antenna design. In addition, second resonance is advantageous because its electric filed distribution along the slot has two maximum points which are ideal locations for capacitive loading. Furthermore, due to the higher operation frequency of second resonance, small changes in the capacitance results in higher reactive loading variations.

Note that, the calculated resonance frequencies using the circuit model are only an approximation, since the effects of radiation, feed network and finite ground size are not considered. The purpose of this model is only to determine the approximate value and the capacitor locations. Therefore, full-wave simulation is used to characterize the exact resonance frequency.

TABLE I
Rate of Change of the Second Resonance Frequency with Respect to the Change in Capacitance for Capacitor Position in te Range of 50 μm–300 μm.

l_1, l_2 (μm)	50	100	150	200	250	300
$\Delta f_{R2}/\Delta C$ (GHz/fF)	0.28	0.93	1.28	1.39	1.38	1.32

B. Radiation Pattern of The Reconfigurable Slot Antenna

The radiation pattern of a slot antenna depends on the the electric field (magnetic current) distribution over its aperture [24], [25]. The slot antenna at its first resonance has a symmetric field distribution, which results in a broadside radiation pattern. On the other hand, at its second resonance, field distribution is anti symmetric which creates null at the

This article has been accepted for publication in a future issue of this journal, but has not been fully edited. Content may change prior to final publication. Citation information: DOI 10.1109/TAP.2021.3102112, IEEE Transactions on Antennas and Propagation

broadside [25]. The bent slot antenna of [26] was designed for the operation in the microwave band with PIN diodes used for the frequency reconfiguration. We have adopted and modified this bent slot design for operation at 100 GHz and reconfiguration using paraffin variable capacitors. Since the antenna is operated at its second resonance, geometry of the antenna is modified as a bent slot. A bending the antenna causes a cancellation of magnetic currents in the bent section, which yields a field distribution similar to the first resonance. Hence, the antenna will have a broadside radiation pattern [25].

III. Full-Wave Simulation of The Reconfigurable Slot Antenna

Geometry of the designed reconfigurable slot antenna is shown in Fig. 4. Bent slot has a width of 80 μm and total length of 1357 μm which is approximately one wavelength at 130 GHz. Antenna substrate is a 200 μm-thick quartz with relative dielectric constant of $\epsilon_r = 3.8$ and loss tangent of 4×10^{-4}. The ground plane of the antenna is 2.2×3.4 mm^2 and it is fabricated with a 750 nm-thick (three times the skin depth at 100 GHz) layer of gold with the conductivity of 4.1×10^7 S/m. Full-wave simulation is performed using ANSYS HFSS.

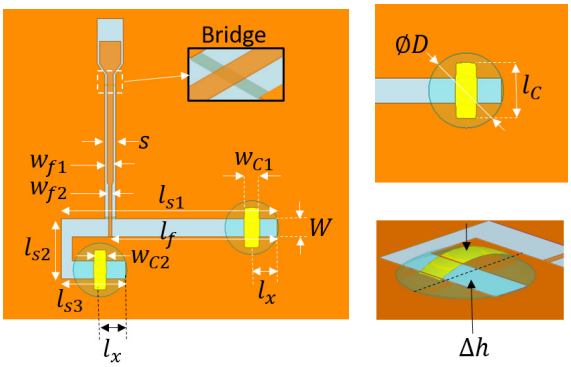

Fig. 4. 3D simulation model of the reconfigurable antenna. Detailed view of the (a) antenna and (b) paraffin PCM capacitor.

The slot antenna is loaded with paraffin PCM capacitors and the PCM device, as shown in Fig. 1, consists of a Joule heater positioned under the ground plane to ensure a minimum electromagnetic coupling to the antenna. The initial thickness of the paraffin is considered as 2.6 μm with a maximum center displacement of 1.2 μm which is determined using multiphysics simulation [23]. The relative dielectric constant and loss tangent of paraffin are 2.55 and 6.3×10^{-4} [19], respectively. Although the approximate values for the capacitance and their locations are calculated in Section II-A, the exact values for the width of capacitor top plate, w_{C1} and w_{C2} are determined using a full-wave simulation, as given in Table II.

The slot antenna is fed through an off-center coplanar waveguide (CPW) transmission line where the input impedance at the feed location is 118 Ω. The antenna is impedance-matched to 50 Ω using a quarter-wave transformer. To avoid parasitic slot line modes at the transition points on the transmission lines, air-bridges are used [28]. These air-bridges are fabricated under the CPW lines and separated by a 1 μm-thick layer of silicon dioxide ($\epsilon_r = 2.2$) rather than being suspended in air. All of the dimensions of the antenna are given in Table II.

TABLE II
Geometric parameters of antennas, capacitors and feed lines in microns.

l_{s1}	l_{s2}	l_{s3}	W	l_f	S	w_{f1}	w_{f2}	w_{ab}
964	268	285	80	746	47	14	27	8

l_x	w_{C1}	w_{C2}	l_C	D	h
113	58	70	200	120	2.6

Fig. 5 shows the simulated return loss of the antenna with respect to the maximum displacement. Total reconfigured antenna bandwidth is 94 GHz–102.2 GHz (S_{11} <-10 dB) and the resonance frequency (minimum of S_{11}) changes by 4.6 GHz. Increasing the displacement results in a decrease in capacitance, which results in a increase in the resonance frequency, as shown in Fig. 6(a). The antenna efficiency at resonance frequency with respect to the displacement is illustrated in Fig. 6(b). It can be observed that, a decrease in resonance frequency also decreases the radiation efficiency as a result of the reduction in the electrical size of the antenna [29]–[31].

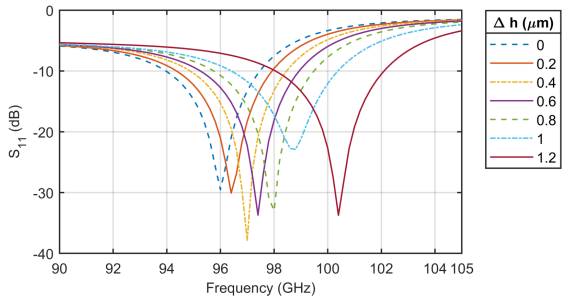

Fig. 5. Simulated S_{11} of the antenna with respect to center displacement of the paraffin PCM capacitor.

A lumped element model is next used to characterize the capacitance and the loss of the paraffin PCM device. Using the full-wave simulation, paraffin PCM capacitors are replaced with lumped ports and 3-port S-parameters of the antenna is determined. Next, S-parameters are imported into a circuit simulator and the series capacitance and resistance are extracted. A plot of the extracted capacitance value versus the input heater voltage is shown in Fig. 6(b). The results of these full-wave and multiphysics simulations resulted in a capacitance change of 15.3% for the maximum displacement of 1.2 μm, which is consistent with the volumetric expansion of the paraffin. The average series resistance of the paraffin PCM capacitor is found to be 610 mΩ.

The simulated radiation pattern of the antenna for the center displacement of 1.2 μm and 0.2 μm are plotted in Fig. 7. Since the current distribution for different displacement values are approximately constant, antenna maintains its bidirectional

This article has been accepted for publication in a future issue of this journal, but has not been fully edited. Content may change prior to final publication. Citation information: DOI 10.1109/TAP.2021.3102112, IEEE Transactions on Antennas and Propagation

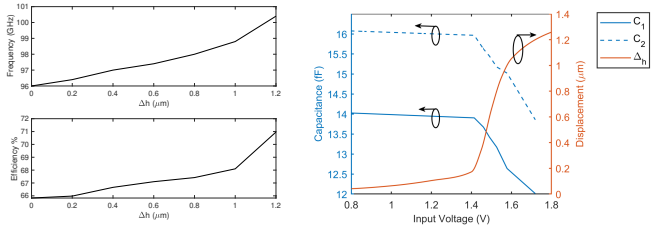

(a) (b)

Fig. 6. (a) Resonance frequency and total efficiency with respect to the center displacement of the capacitor. (b)Capacitance change and maximum center displacement of the paraffin PCM capacitor for various input voltage.

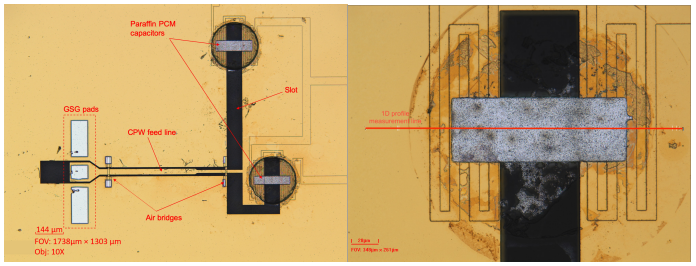

(a) (b)

Fig. 8. Micrograph of the fabricated (a) reconfigurable slot antenna and (b) the paraffin PCM capacitor.

pattern and has a maximum realized gain of 3 dBi at 100 GHz.

IV. Experimental Results

Antenna integrated with paraffin PCM capacitors are fabricated using six-layer photolithography process as described in [23]. Note that, the fabrication paraffin PCM actuator is compatible with surface micromachining processes that can be implemented similar to the conventional MEMS process. A micrograph of the fabricated antenna and the paraffin PCM capacitor is shown in Fig. 8.

3D profile measurement results of the mechanical displacement of the paraffin actuator is illustrated in [23] where the maximum displacement at the center of the device to be 1.4 μm with an initial paraffin film thickness of 2.6 μm. Moreover, based on the transient multiphysics simulation, switching time to actuate the device is 5.7 ms [23] .

Using a ground-signal-ground (GSG) mmW probe, input impedance of the antenna is characterized. Based on this measurement, reconfiguration capability and the RF performance of paraffin PCM capacitor is evaluated. Our measurement setup consists of a waveguide probe (Form Factor Inc.) connected to a frequency extender (Virginia Diodes Inc.), combined with a PNA (Keysight N5242A). Frequency range of the setup is limited to 90–140 GHz. A probe station was used for the experiments with a 30 mm-thick foam layer to isolate the wafer from the metallic chuck (see Fig. 9 for an illustration of this measurement configuration). Foam layer is approximately 10λ-thick which minimizes the effect of the metallic chuck on the impedance of the antenna.

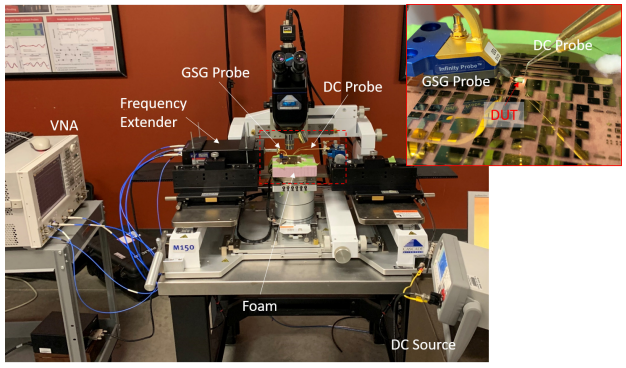

Fig. 9. mmW measurement setup. Close-up view of the probes and the device under test (DUT) is shown in the inset.

One port Calibration is performed in two steps. Initially, the network analyzer is calibrated to a reference plane at the output of the frequency extender. Short, $\lambda/8$-delayed short and load standards are used for this calibration. After attaching the probe to the waveguide port, system is calibrated to the reference place at the tip of the probe. Calibration is performed using on-wafer, four CPW offset shorts [36]. The CPW dimensions are 10/96/10 μm and the length of the lines are determined using established methods in [37], [38]. A micrograph of the calibration standards is shown in Fig. 10. For the first short, contact point of the probe is 350 μm away from the shorting plane to minimize the effect of the probe-CPW discontinuity, with the probe pads are designed to match the 100-μm probe pitch. The short standards have a delay length difference of 200 μm that correspond to 83° at 110 GHz.

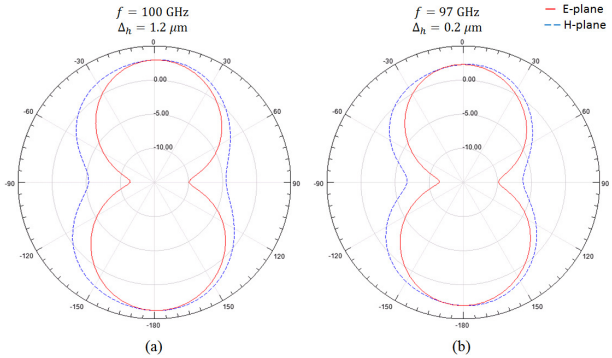

(a) (b)

Fig. 7. Principal plane patterns of the reconfigurable antenna for the center displacement of (a) 1.2 μm at 100 GHz and (b) 0.2 μm at 97 GHz.

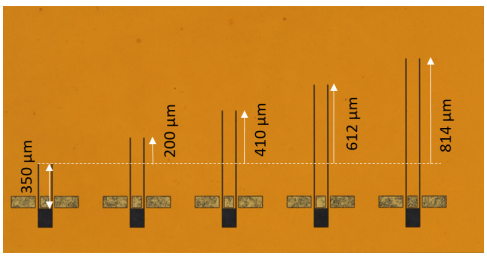

Fig. 10. Micrograph of the CPW offset short calibration standards.

This article has been accepted for publication in a future issue of this journal, but has not been fully edited. Content may change prior to final publication. Citation information: DOI 10.1109/TAP.2021.3102112, IEEE Transactions on Antennas and Propagation

TABLE III
COMPARISON OF MMW RECONFIGURABLE ANTENNAS IN LITERATURE

Reference	Reconfiguring element	No. of elements	No. of states	Variable change (%)	Frequency range	Frequency shift
[32]	PIN diode switched capacitor	1	Discrete	Capacitance, 59% (63–100 fF)	27.8–28.8 GHz	1 GHz
[33]	Schottky varactor	1	Continuous	Capacitance, 100% (2.4–4.79 fF)	202.7–197 GHz	5.7 GHz
[34]	Pneumatic actuator	1	Continuous	Displacement, 187%, (200–573 μm)	51–55.3 GHz	4.3 GHz
[10]	RF-MEMS	2	4	N/A	28, 29.2, 31.5, 35 GHz	7 GHz
[35]	Photoconductive switch	4	2	N/A	30, 34 GHz	4 GHz
This work	Paraffin PCM Capacitor	2	Continuous	Capacitance, 15%	94.3–101.6 GHz	7.3 GHz

Both PCM capacitors are excited by applying DC voltage of 1–6 V to heaters in series configuration. DC voltage is supplied using a DC source (Keysight B2901A) via separate probes. Reflection coefficient of the antenna is measured for various heater voltages. The arrangement of the probes are shown in the inset of Fig. 9.

The antenna reflection coefficient with an input voltage of zero yields an antenna resonance frequency of 94.6 GHz, as shown in Fig. 11(a). Using the lumped element model based on the full-wave simulation (described in Section III) , it is calculated that $C_1 = 17.8$ fF and $C_2 = 25.3$ fF with an estimated resistance value of 4.4 Ω. Measured resistance values are significantly higher than the simulated value of 610 mΩ given in Section III. Increased resistance could be due to extreme rough surface and the variation of the thickness of the fabricated aluminum layer. In addition, losses in the simulated antenna model could be underestimated, in this case contribution of the all of the losses are reflected in the PCM capacitors. To actuate the capacitors, 5.4 V is applied to the heaters and the reflection coefficient of the antenna is shown in Fig. 11(b). Extracted capacitance values are $C_1 = 13.4$ fF and $C_2 = 17.4$.

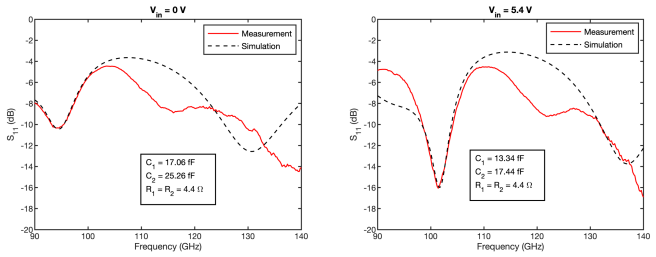

(a) (b)

Fig. 11. Comparison of the simulated and measured S_{11} of the antenna for heater voltage of (a) 0 V and (b) 5.4 V.

Fig. 12(a) shows the S_{11} of the antenna for input heater voltage of 0–5.4 V. Antenna cover the bandwidth of 94.1–104.1 GHz. In Fig. 12(b), Resonance frequency is shown as a function of voltage of the heater. Resonance frequency increases monotonically from 94.3 GHz to 101.6 GHz. As the voltage increases from 3.8 to 4 V, we observe a rapid increase in the resonance frequency which is associated with phase transition of the paraffin. Based on the multiphysics simulation, by controlling the input voltage of the heater, finer tuning can be achieved. However, since the current design does not include any packaging, temperature distribution of the capacitor is highly dependent on the ambient.

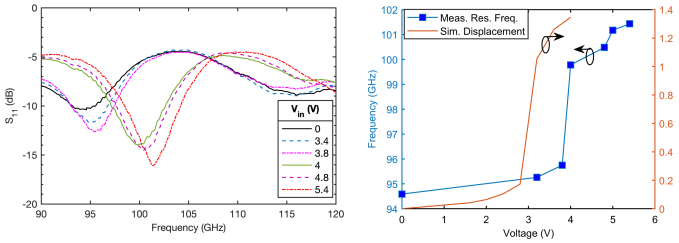

(a) (b)

Fig. 12. Measured (a) reflection coefficient and (b) resonance frequency (frequency of maximum return loss) of the antenna and the simulated displacement of the paraffin PCM capacitor with respect to the input voltage of te heater [23].

A comparison of our novel design with state-of-art mmW reconfigurable antennas from literature is given in Table III. It can be observed that the paraffin PCM based reconfigurable antenna can achieve a reconfiguration range of 7.3 GHz with a relatively small capacitance change of 15%.

V. CONCLUSION

A continuously reconfigurable mmW slot antenna using paraffin PCM variable capacitors was designed, fabricated and tested. To achieve reconfiguration, a bent slot antenna is loaded with two PCM variable capacitors. This work, is the first implementation of a mmW reconfigurable antenna using a class of electrothermally actuated capacitor based on the paraffin phase change materials which is capable of operation at 100 GHz. Unique combination of low dielectric loss and large temperature dependent density change of paraffin, facilitate the development of low loss reconfigurable structures at mmW band. In contrast to the classical RF-MEMS devices, paraffin PCM variable capacitors offers continuous tuning with a similar low-loss performance with a series resistance of less than 0.7 Ω at 100 GHz.

Using on-wafer probe measurements it was shown that the designed reconfigurable antenna covers the bandwidth of 94.1–104.1 GHz and the resonance frequency shifts from 94.3 GHz to 101.6 GHz with the increasing heater voltage. In addition, capacitance change of the paraffin PCM devices are calculated to be 15.3% for a measured maximum displacement of 1.34 μm. Antenna has a simulated maximum gain of 3 dBi. A good agreement is observed between the simulation and measurement results for both electromagnetic performance of the antenna and displacement of the capacitor.

REFERENCES

[1] B. He and H. Jafarkhani, "Low-complexity reconfigurable MIMO for millimeter wave communications," *IEEE Transactions on Communications*, vol. 66, no. 11, pp. 5278–5291, 2018.

[2] D. Peroulis, K. Sarabandi, and L. P. B. Katehi, "Design of reconfigurable slot antennas," *IEEE Transactions on Antennas and Propagation*, vol. 53, no. 2, pp. 645–654, Feb 2005.

[3] S. Genovesi, A. D. Candia, and A. Monorchio, "Compact and low profile frequency agile antenna for multistandard wireless communication systems," *IEEE Transactions on Antennas and Propagation*, vol. 62, no. 3, pp. 1019–1026, March 2014.

[4] Y. P. Selvam, L. Elumalai, M. G. N. Alsath, M. Kanagasabai, S. Subbaraj, and S. Kingsly, "Novel frequency- and pattern-reconfigurable rhombic patch antenna with switchable polarization," *IEEE Antennas and Wireless Propagation Letters*, vol. 16, pp. 1639–1642, 2017.

[5] H. Sun and Z. Pan, "Design of a quad-polarization-agile antenna using a switchable impedance converter," *IEEE Antennas and Wireless Propagation Letters*, vol. 18, no. 2, pp. 269–273, Feb 2019.

[6] F. Farzami, S. Khaledian, B. Smida, and D. Erricolo, "Pattern-reconfigurable printed dipole antenna using loaded parasitic elements," *IEEE Antennas and Wireless Propagation Letters*, vol. 16, pp. 1151–1154, 2017.

[7] C. R. White and G. M. Rebeiz, "Single- and dual-polarized tunable slot-ring antennas," *IEEE Transactions on Antennas and Propagation*, vol. 57, no. 1, pp. 19–26, Jan 2009.

[8] T. Aboufoul, A. Alomainy, and C. Parini, "Reconfiguring UWB monopole antenna for cognitive radio applications using GaAs FET switches," *IEEE Antennas and Wireless Propagation Letters*, vol. 11, pp. 392–394, 2012.

[9] B. Ahn, H. Jo, J. Yoo, J. Yu, and H. L. Lee, "Pattern reconfigurable high gain spherical dielectric resonator antenna operating on higher order mode," *IEEE Antennas and Wireless Propagation Letters*, vol. 18, no. 1, pp. 128–132, Jan 2019.

[10] K. Van Caekenberghe and K. Sarabandi, "A 2-bit Ka-band RF MEMS frequency tunable slot antenna," *IEEE Antennas and Wireless Propagation Letters*, vol. 7, pp. 179–182, 2008.

[11] O. H. Karabey, S. Bildik, S. Bausch, S. Strunck, A. Gaebler, and R. Jakoby, "Continuously polarization agile antenna by using liquid crystal-based tunable variable delay lines," *IEEE Transactions on Antennas and Propagation*, vol. 61, no. 1, pp. 70–76, Jan 2013.

[12] S. Bildik, S. Dieter, C. Fritzsch, W. Menzel, and R. Jakoby, "Reconfigurable folded reflectarray antenna based upon liquid crystal technology," *IEEE Transactions on Antennas and Propagation*, vol. 63, no. 1, pp. 122–132, Jan 2015.

[13] K. K. Karnati, M. E. Trampler, and X. Gong, "A monolithically BST-integrated K_α -band beamsteerable reflectarray antenna," *IEEE Transactions on Antennas and Propagation*, vol. 65, no. 1, pp. 159–166, 2017.

[14] S. Srivastava, J. Handoo, K. Agrawal, and G. Joshi, "Phase-transition studies in n-alkanes and petroleum-related waxes—a review," *Journal of Physics and Chemistry of Solids*, vol. 54, no. 6, pp. 639–670, 1993.

[15] S. Himran, A. Suwono, and G. A. Mansoori, "Characterization of alkanes and paraffin waxes for application as phase change energy storage medium," *Energy Sources*, vol. 16, no. 1, pp. 117–128, 1994.

[16] E. T. Carlen and C. H. Mastrangelo, "Surface micromachined paraffin-actuated microvalve," *Journal of Microelectromechanical Systems*, vol. 11, no. 5, pp. 408–420, 2002.

[17] M. Lehto, R. Boden, U. Simu, K. Hjort, G. Thornell, and J. Schweitz, "A polymeric paraffin microactuator," *Journal of Microelectromechanical Systems*, vol. 17, no. 5, pp. 1172–1177, 2008.

[18] R. Boden, M. Lehto, U. Simu, G. Thornell, K. Hjort, and J.-A. Schweitz, "A polymeric paraffin actuated high-pressure micropump," *Sensors and Actuators A: Physical*, vol. 127, no. 1, pp. 88–93, 2006.

[19] B. Ghassemiparvin and N. Ghalichechian, "Complex permittivity measurement of paraffin phase-change material at 26 GHz–1.1 THz using time-domain spectroscopy," *Journal of Infrared, Millimeter, and Terahertz Waves*, vol. 40, no. 2, pp. 210–218, Feb 2019.

[20] B. Ghassemiparvin and N. Ghalichechian, "Reconfigurable millimeter-wave antennas using paraffin phase change materials," in *2016 10th European Conference on Antennas and Propagation (EuCAP)*, April 2016, pp. 1–4.

[21] B. Ghassemiparvin, S. Shah, and N. Ghalichechian, "Novel paraffin-based 100-GHz variable capacitors for reconfigurable antennas," in *2017 11th European Conference on Antennas and Propagation (EuCAP)*, March 2017, pp. 3506–3510.

[22] B. Ghassemiparvin and N. Ghalichechian, "Paraffin-based RF microsystems for millimeter wave reconfigurable antennas," in *2019 IEEE International Symposium on Antennas and Propagation USNC/URSI National Radio Science Meeting*, July 2019.

[23] ——, "Paraffin-based reconfigurable antenna operating at 100 GHz," *Journal of Microelectromechanical Systems*, vol. 29, no. 5, pp. 621–628, 2020.

[24] R. Garg, P. Bhartia, I. Bahl, and A. Ittipiboon, *Microstrip Antenna Design Handbook*, ser. Antennas and Propagation Library. Artech House, 2001.

[25] N. Behdad and K. Sarabandi, "A varactor-tuned dual-band slot antenna," *IEEE Transactions on Antennas and Propagation*, vol. 54, no. 2, pp. 401–408, Feb. 2006.

[26] ——, "Dual-band reconfigurable antenna with a very wide tunability range," *IEEE Transactions on Antennas and Propagation*, vol. 54, no. 2, pp. 409–416, Feb. 2006.

[27] D. Pozar, *Microwave Engineering, 4th Edition*. Wiley, 2011.

[28] R. Simons, *Coplanar Waveguide Discontinuities and Circuit Elements*. John Wiley & Sons, Ltd, 2002.

[29] L. J. Chu, "Physical limitations of omni-directional antennas," *Journal of Applied Physics*, vol. 19, no. 12, pp. 1163–1175, 1948.

[30] R. F. Harrington, "Effect of antenna size on gain, bandwidth, and efficiency," *Journal of Research of the National Bureau of Standards. Section D: Radio Propagation*, vol. 64D, no. 1, p. 1, 1960.

[31] R. C. Hansen, "Fundamental limitations in antennas," *Proceedings of the IEEE*, vol. 69, no. 2, pp. 170–1–82, Feb 1981.

[32] J. Choi, J. Park, Y. Youn, W. Hwang, H. Seong, Y. N. Whang, and W. Hong, "Frequency-adjustable planar folded slot antenna using fully integrated multithrow function for 5g mobile devices at millimeter-wave spectrum," *IEEE Transactions on Microwave Theory and Techniques*, vol. 68, no. 5, pp. 1872–1881, 2020.

[33] Z. Jiang, S. M. Rahman, P. Fay, J. L. Hesler, and L. Liu, "Tunable 200 GHz lens-coupled annular-slot antennas using schottky varactor diodes for all-electronic reconfigurable terahertz circuits," *Electronics Letters*, vol. 49, no. 23, pp. 1428–1430, 2013.

[34] S. Hage-Ali, N. Tiercelin, P. Coquet, R. Sauleau, V. Preobrazhensky, and P. Pernod, "A millimeter-wave inflatable frequency-agile elastomeric antenna," *IEEE Antennas and Wireless Propagation Letters*, vol. 9, pp. 1131–1134, 2010.

[35] I. F. da Costa, A. Cerqueira S., D. H. Spadoti, L. G. da Silva, J. A. J. Ribeiro, and S. E. Barbin, "Optically controlled reconfigurable antenna array for mm-wave applications," *IEEE Antennas and Wireless Propagation Letters*, vol. 16, pp. 2142–2145, 2017.

[36] J. P. Dunsmore, *Handbook of Microwave Component Measurements*. John Wiley & Sons, Ltd, 2012.

[37] L. Chen, C. Zhang, T. J. Reck, A. Arsenovic, M. Bauwens, C. Groppi, A. W. Lichtenberger, R. M. Weikle, and N. S. Barker, "Terahertz micromachined on-wafer probes: Repeatability and reliability," *IEEE Transactions on Microwave Theory and Techniques*, vol. 60, no. 9, pp. 2894–2902, Sep. 2012.

[38] Anritsu Company, *Understanding VNA Calibration*, 2012 (accessed November 30, 2019).